Develop dissipative particle dynamics method to study the fluid flow and heat transfer of Ar and O_2 flows in the micro- and nanochannels with precise atomic arrangement versus molecular dynamics approach

Abdolmajid Taghipour, Arash Karimipour, Masoud Afrand, Somaye Yaghoubi & Mohammad Akbari

Journal of Thermal Analysis and Calorimetry
An International Forum for Thermal Studies

ISSN 1388-6150
Volume 144
Number 6

J Therm Anal Calorim (2021)
144:2575-2586
DOI 10.1007/s10973-020-10329-2

Springer

Journal of Thermal Analysis and Calorimetry (2021) 144:2575–2586
https://doi.org/10.1007/s10973-020-10329-2

Develop dissipative particle dynamics method to study the fluid flow and heat transfer of Ar and O_2 flows in the micro- and nanochannels with precise atomic arrangement versus molecular dynamics approach

Abdolmajid Taghipour[1] · Arash Karimipour[1] · Masoud Afrand[1] · Somaye Yaghoubi[1] · Mohammad Akbari[1]

Received: 31 August 2020 / Accepted: 3 October 2020 / Published online: 29 October 2020

Abstract
Fluid atomic behavior is an important factor for industrial applications. Computer simulations based on simple models predict Poiseuille flow for these atomic structures with the presence of external force. In this work, we describe the dynamical properties of Ar and O_2 flows with precise atomic arrangement via dissipative particle dynamics (DPD) and molecular dynamics (MD) simulation approaches. In these methods, each model is represented by using Large-scale Atomic/Molecular Massively Parallel Simulator package. Simulation results show that maximum rate for velocity of Ar flow in platinum and copper microchannels is 0.100 (unit less)/0.091 Å ps^{-1} and 0.121 (unit less)/0.105 Å ps^{-1} by using DPD/MD approach. This atomic parameter changes to 0.111 (unit less)/0.102 Å ps^{-1} and 0.125 (unit less)/0.108 Å ps^{-1} for O_2 fluid with mentioned approaches. By decreasing the microchannel size, the maximum rate of velocity reaches to 0.101 (unit less)/0.099 Å ps^{-1} and maximum temperature rate decreases to 485 (unit less)/440 K with DPD/MD approaches. These calculated parameters can be used in industrial application designing for some processes such as heat transfer in structures. It was seen that the developed DPD approach was able to simulate the fluid flow and heat transfer of various types of fluids at micro- and nanoscales with suitable accuracy versus MD.

Keywords Dissipative particle dynamics (DPD) · Molecular dynamics (MD) · Microchannel · Nanochannel

Introduction

Fluid analyzing in various channels at atomic scales is a challenging procedure because of the difficulty of particles interaction [1–7]. In principle, molecular dynamics (MD) method can be used to exactly describe the various structures and fluids, but it is computationally heavy process. In this method, as a result of interaction between atoms, an insight into the time evolution of the whole atomic system is gained. For computations of the atom's motion through time, Newton's second law at the atomic level is used as the gradient of the interatomic potential function. This computational method is used for various fluid study by atomic accuracy. Zheng et al. [8] simulated the nanofluid thermal and atomic behavior in non-ideal channel. Results of this study show the molecular dynamics of good accuracy for fluids simulation. Mosavi et al. [9] reported the Poiseuille water based-nanofluid flows in nanochannels. The results of this research show the importance of nanochannels atomic arrangement in nanofluid behavior. Asgari et al. [10] simulated the H_2O fluid and H_2O/Cu nanofluid in atomic microchannel and show the Poiseuille manner of them in presence of external force. Various methods such as lattice Boltzmann and finite volume approaches have been introduced for studying fluid behavior in various channels [11–14]. These methods have been utilized with some success to simulate various microscale phenomena [15, 16]. Dissipative particle dynamics (DPD) method is another numerical approach to simulate the common fluid dynamical behavior. Technically, DPD particle can be assumed as a group of atoms or molecules. Macroscopic conservation equations can be gained from the DPD equations of motion [17–19]. Hence, DPD computational method can be used for continuum

✉ Arash Karimipour
arashkarimipour@gmail.com

[1] Department of Mechanical Engineering, Najafabad Branch, Islamic Azad University, Najafabad, Iran

structures. This makes DPD approach a powerful method for describing the various phenomena. For example, this computational method has been successfully employed to simulate various fluids [20–23]. DPD method is also utilized for the simulation of multiphase structures at microscales [24, 25]. Moreover, other works can be addressed in this way, involving the fluid particles effects through the hydrodynamic and thermal flow properties. Borhani et al. [26] simulated the heat transfer process in a channel with parallel plates by using DPD approach with energy conservation. The results of this computational research show the DPD method ability in description of thermal and atomic behavior of fluids. Waheed et al. [27] used DPD approach to model the trajectories of micro-objects in a practical microfluidic device. The researchers in this computational work achieved to high computational speed and accuracy by adjusting the DPD parameters, such as force coefficients, thermal energies of the particles, and time steps. By studying the previous reports [28–38], we use MD and DPD computational methods to simulate atomic manner of O_2/Ar fluid in Pt and Cu microchannels in this work. Finally, the results of these two approaches were compared with each other to estimate the accuracy of these computational methods. In summary, computational study in this work consists of two main steps:

Step a Equilibrium Process of Fluid-Channel Structure: Ar/O_2 fluid and Pt/Cu channels were simulated in the simulation box with $l_x = l_y/4 = l_z/4$ lengths. Periodic boundary conditions were implemented in x direction and fix one used for y and z directions.

Step b Atomic Manner of Fluid-Channel Structure: In the second step, the density, velocity, and temperature profiles of simulated fluid were calculated in the simulation box by adding external force to fluid particles (Ar and O_2), and dynamical behavior of simulated fluids in Pt/Ar channels was reported.

Computational method

MD computational method is the common type of atomic simulation that is enabled to describe the dynamical behavior of various structures [39–41]. This approach is used in the atomic manner study of nano-structures [42–47]. Newton's second law at the atomic level,

$$F_i = \sum_{i \neq j} F_{ij} = m_i \frac{d^2 r_i}{dt^2} = m_i \frac{dv_i}{dt} \tag{1}$$

$$F_i = -\sum \text{grad}\, V_{ij}(r_{ij}) \tag{2}$$

$$\frac{3}{2} k_B T = \frac{1}{N_{atom}} \sum_{i=1}^{N} \frac{1}{2} m v_i^2 \tag{3}$$

The instantaneous temperature fluctuates are obtained by the Eq. (4),

$$T(t) = \sum_{i}^{N} \frac{m_i v_i^2(t)}{k_B N_{sf}} \tag{4}$$

where N_{sf} is the degree of freedom of the atomic structure. Lennard–Jones (LJ) formalism:

$$U(r) = 4\varepsilon \left[\left(\frac{\sigma}{r_{ij}} \right)^{12} - \left(\frac{\sigma}{r_{ij}} \right)^{6} \right] \quad r \ll r_c \tag{5}$$

Potential coefficient from UFF potential is reported in Table 1.

In UFF interatomic potential, the bonded interactions are described by harmonic formalism. Embedded Atom Model (EAM) potential is represented by Eq. (5) [48]:

$$E_i = F_{\alpha}\left(\sum_{i \neq j} \rho_{\beta}(r_{ij}) \right) + \frac{1}{2} \sum_{i \neq j} \phi_{\alpha\beta}(r_{ij}) \tag{6}$$

In this equation, r_{ij} is the distance between atoms i and j, $\phi_{\alpha\beta}$ is a pairwise potential function, $\rho_{\alpha\beta}$ is the contribution to the electron charge density from atom j of type β at the location of atom i, and F_{α} is an embedding function that represents the energy required to place atom i of type α into the electron cloud. After atomic modeling of each structure, the equations of motion are calculated at initial condition. Association of motion equations is fulfilled by velocity-Verlet algorithm for integrating the Newton's law that is shown as follows:

$$v(t + t\delta) = v(t) + a(t)\delta t \tag{7}$$

$$r(t + t\delta) = r(t) + v(t)\delta t \tag{8}$$

where $r(t + t\delta)$ and $v(t + t\delta)$ refer to coordinate and velocity of particles and $r(t)$,$v(t)$ refer to the first rate of these parameters, respectively. These MD simulations are done by LAMMPS simulation package in metal model, and the physical parameter units in this model are represented in Table 2 [49–52].

Table 1 The length and energy parameters for LJ potential in our MD simulations [46]

Element	σ/Å	ε/eV
Ar	3.868	0.00802
O	3.500	0.00009
Pt	2.754	0.00347
Cu	3.495	0.00022

Table 2 The physical parameters units in metal model of LAMMPS package

Metal	Model
Units	Quantity
g/mole	Mass
Å	Distance
ps	Time
eV	Energy
Å/ps	Velocity
eV/Å	Force
K	Temperature
Bars	Pressure
multiple of electron charge	Charge

In the second phase of this work, we use DPD approach to study the fluid behavior. DPD is a computational approach to study the dynamic properties of various structures. It was introduced by Hoogerbrugge and Koelman to avoid the lattice artifacts of the so-called lattice gas automata [53, 54]. Later, it was optimized by P. Espanol to ensure the appropriate equilibrium state [55, 56]. The algorithms presented in these groups choose randomly a pair particle for applying DPD thermostating. Computationally, DPD is an effective simulation approach which involves a group of particles displace in defined region. In this method, the total force which is acting on a particle i is given by a sum over all particles j that lie within a defined cutoff distance of three pairwise additive forces [57]:

$$F_{\mathrm{i}} = \sum_{\mathrm{j}\neq\mathrm{i}} \left(F_{\mathrm{ij}}^{\mathrm{C}} + F_{\mathrm{ij}}^{\mathrm{D}} + F_{\mathrm{ij}}^{\mathrm{R}}\right) \tag{9}$$

In this equation, the first term is a conservative force, the second is a dissipative force, and the third is a random force, respectively. All parameters in Eq. (6) are unit less. The conservative term in this equation acts to give beads a chemical identity, while the dissipative and random terms equilibrate the temperature of simulated structure. An important property of all of the nonbonded forces is that they conserve momentum, so that hydrodynamic modes of the simulated structures are detectable for small particle numbers [58–60]. The results obtained from DPD simulations highly depend on the choice of the potential function as MD simulations. In order to get correct results, one should choose the potential function based on the physical properties. In this potential function, the force on atom i due to atom j is given as a sum of three terms:

$$f = \left(F^{\mathrm{C}} + F^{\mathrm{D}} + F^{\mathrm{R}}\right) r_{\mathrm{ij}}, \quad r < r_{\mathrm{c}} \tag{10}$$

$$F^{\mathrm{C}} = A\omega(r) \tag{11}$$

$$F^{\mathrm{D}} = -\gamma\omega^2(r)\left(r_{\mathrm{ij}}.v_{\mathrm{ij}}\right) \tag{12}$$

$$F^{\mathrm{R}} = \sigma\omega(r)\alpha(\Delta t)^{-1/2} \tag{13}$$

$$\omega(r) = 1 - r/r_{\mathrm{c}} \tag{14}$$

Computationally, in our DPD simulations, the simulation box lengths are $30\times30\times90$ and periodic boundary condition is used for x and y directions and fix one implemented to z direction for the first time [61–75]. All the present DPD simulations were provided by LAMMPS. Further, Open Visualization Tool (OVITO) software is used for visualization of our simulations [76]. The initial schematic of fluid and channel arrangement is depicted by OVITO software in Fig. 1.

Results and discussion

Equilibrium process in fluid-channel structure

Temperature and total energy of structures are important physical parameters in MD and DPD simulations. In our simulations, the initial temperatures of particles are set at 300 (temperature unit) by using of NPT ensemble for 2,500,000 time steps. From Figs. 2 and 3, we can say that the temperature rate of Ar particles converged to 300 after equilibrium phase of simulations and so all physical parameters in this computational study reported after 2,500,000 time steps. For O_2 fluid, similar results are calculated as reported in Table 3. Physically, the temperature convergence in structures indicates the limited oscillation of particles in which this oscillation is appropriate with the temperature. Total energy of structures is another important physical parameter that equals the kinetic and potential energies of particles. Figs. 4 and 5 show the total energy of Ar/O_2 fluid convergence with DPD/MD simulation. Numerically, this atomic parameter convergence to −403/−332 (unit less) and −951/−885 eV with DPD and MD approach. Physically, by total energy convergence, the amplitude of simulated structures reaches to a minimum rate. This atomic behavior show the stability of structures and computationally arises from appropriate selection of initial atomic position and interatomic force-fields. Table 3 shows the total energy convergence of Ar and O_2 fluids with various approaches. These computational results show that this parameter of fluid particles in Pt microchannel has bigger rate and so the interatomic interaction between fluid particles is bigger

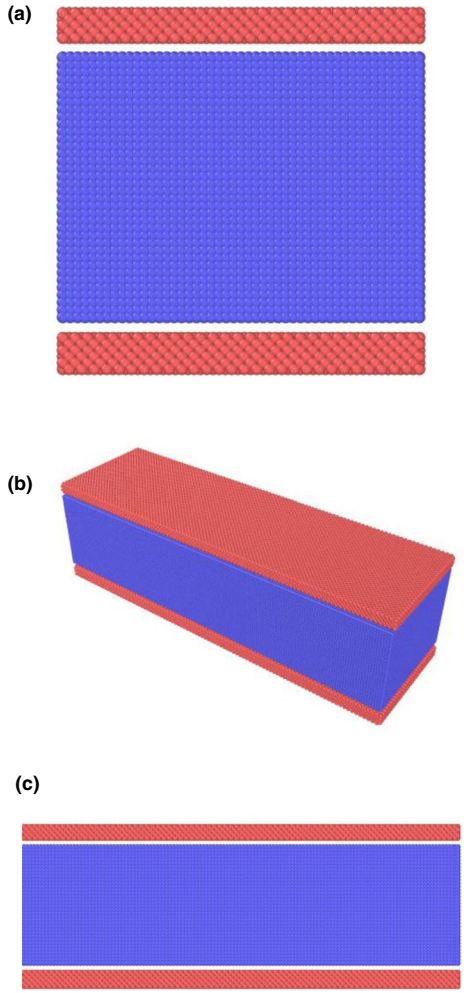

Fig. 1 Schematic of simulated structure with LAMMPS package at **a** Top, **b** Perspective, and **c** Front views

than Cu microchannel. By increasing the total energy of structures, the stability of them increases. Similar physical results calculated for Pt/Cu nanochannels with lower sizes are reported in Table 4.

Density profile of atomic structures

After 2,500,000 time steps, we implemented external force to simulated particles. For report of fluid density profile in our simulations, we divided microchannel/nanochannel to 183 bins and reported the time averaging rate of density under NVE ensemble. The density profiles of Ar/O_2 fluid indicate that the particles are attracted with the walls of channels. Physically, the force between wall and fluid particles is attractive in which this atomic behavior causes density rate to reach a maximum value. Figures 6 and 7 show the density profile of Ar/O_2 fluid in the various

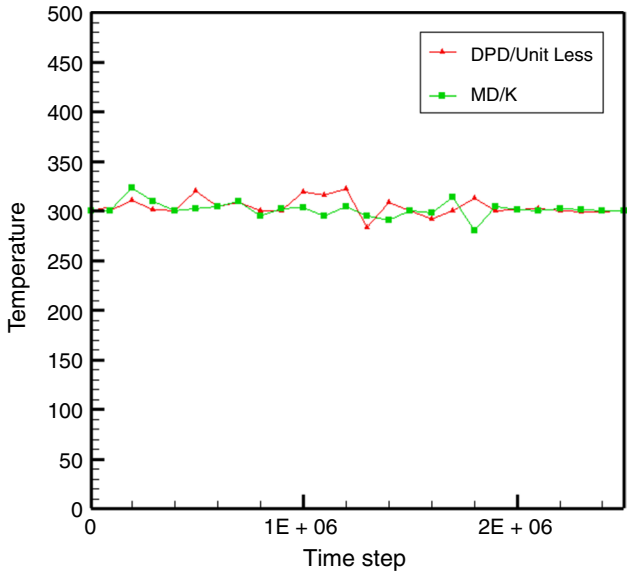

Fig. 2 Temperature of Ar fluid in Pt microchannel

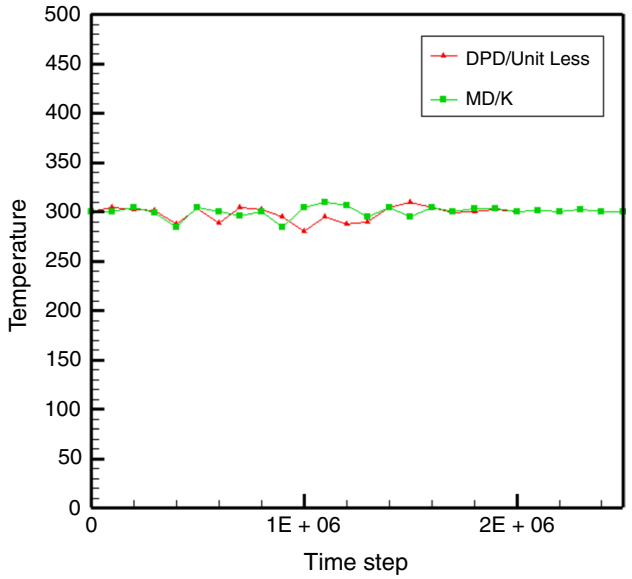

Fig. 3 Temperature of Ar fluid in Cu microchannel

Table 3 The final rate of Ar/O_2 fluid total energy in Pt and Cu microchannels

	Pt microchannel	Cu microchannel
O_2 fluid-MD/eV	−885	−555
O_2 fluid-DPD/Unit less	−332	−223
Ar fluid-MD/eV	−951	−691
Ar fluid-DPD/Unit less	−403	−258

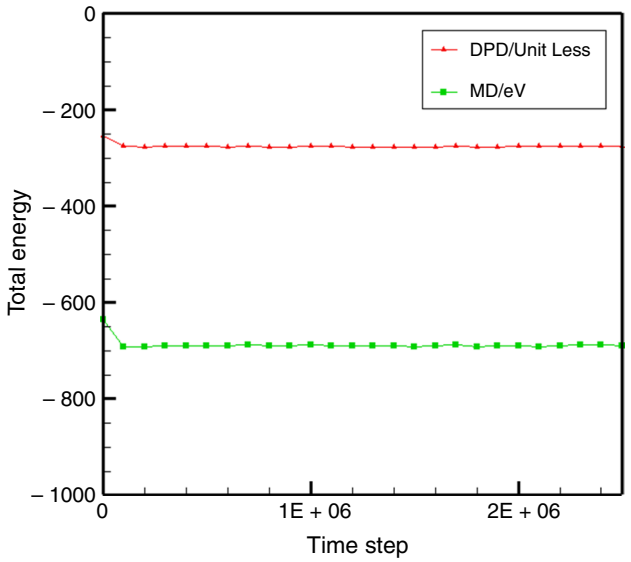

Fig. 4 Total energy of Ar fluid in Pt microchannel

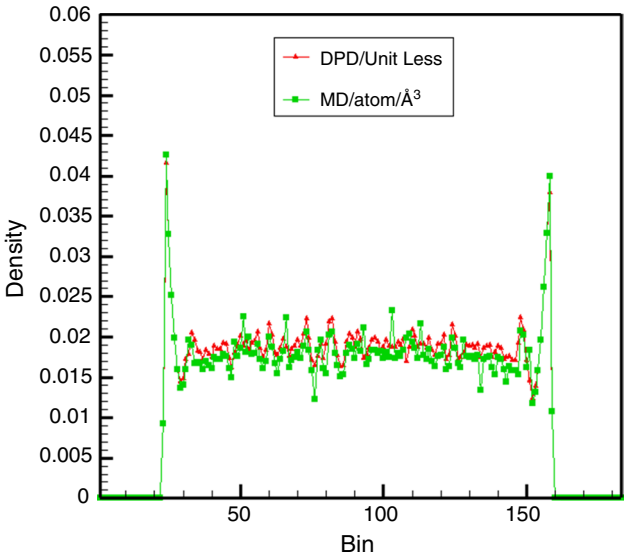

Fig. 6 Density profile of Ar fluid in Pt microchannel

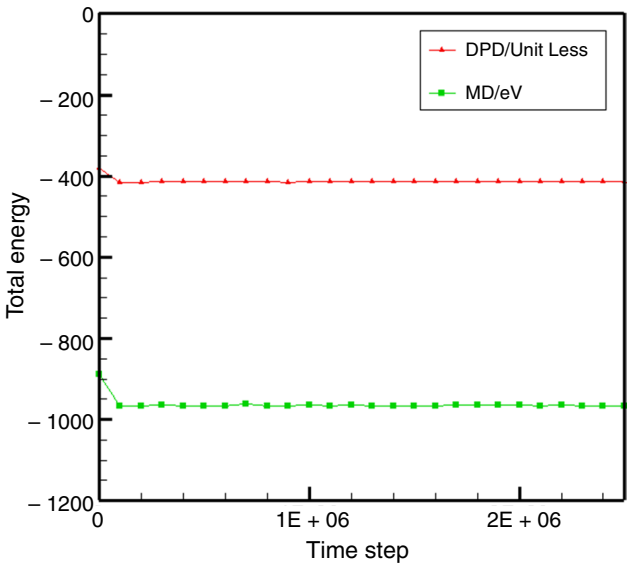

Fig. 5 Total energy of Ar fluid in Cu microchannel

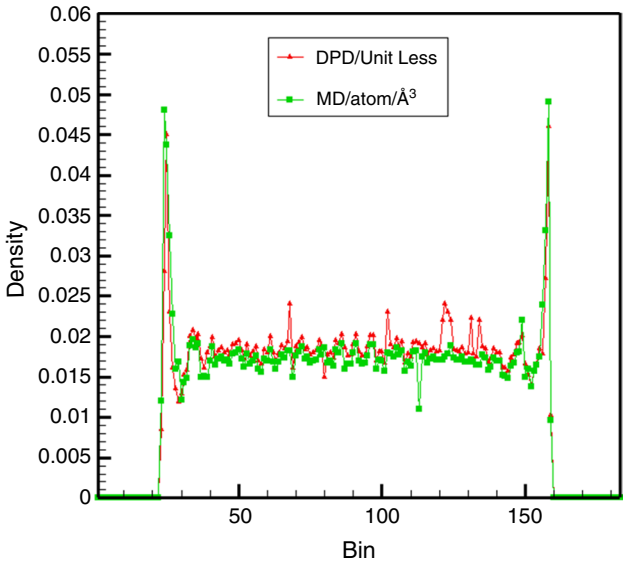

Fig. 7 Density profile of Ar fluid in Cu microchannel

Table 4 The final rate of Ar/O_2 fluid total energy in Pt and Cu nanochannels

	Pt nanochannel	Cu nanochannel
O_2 fluid-MD/eV	−871	−512
O_2 fluid-DPD/Unit less	−312	−203
Ar fluid-MD/eV	−912	−680
Ar fluid-DPD/Unit less	−387	−245

microchannels. From this figure, we can say that the Ar/O_2 atoms are absorbed by metallic walls and this attraction decreases in the middle region of microchannel. Physically, in this simulation region, the fluid atoms interacted with each other and so the atomic positions of them fluctuate relative to an average value. So we conclude that DPD and MD computational methods estimate Poiseuille flow for Ar/O_2 base fluid. These atomic calculations are consistent with previous reports and show validity of our simulation method [77–79]. In microchannel, the attraction force which is implemented to fluid from Pt particles is bigger than Cu

one. Numerically, maximum rate of Ar fluid particles density reaches to 0.046/0.049 atom $Å^{-3}$ in Pt microchannel with DPD/MD method. Industrially, we can conclude that the atomic fluids can be more disrupted in Pt structures. This atomic disruption cause reduces the efficiency of target processes such as heat transfer in micro/nano-structures. Furthermore, from these calculated profiles, we conclude that DPD and MD approaches can describe fluid manner in microchannels appropriately. By size decreasing and converting microchannel to nanochannel, general properties of fluids are repeated. As reported in Tables 5 and 6, the maximum rate of Ar/O_2 density decreases to 0.036/0.038 and 0.024/0.028 atom $Å^{-3}$ rates with DPD and MD approaches. These two methods show that density profiles of fluids fluctuate around the mean rate in middle region of Pt/Cu nanchannels.

Velocity profile of atomic structures

The velocity profiles of Ar/O_2 fluid are calculated in this section. This profile shows the fluid dynamical manner in simulated channels. Physically, velocity of each atom depends on mobility of them and so net force which is inserted in these particles is important. Figure 8 shows the velocity distribution of Ar fluid in Pt microchannel. From this figure, the velocity rate has a minimum rate at 25 and 158 bins in microchannel. Further, we conclude that by getting farther from simulated channel walls, the rate of this atomic parameter increases. As depicted in Fig. 9, DPD and MD computational methods estimate Poiseuille flow for Ar/O_2 base fluid in the presence of external force. Physically, this dynamical manner occurs because of strong atomic interaction between microchannel and fluid atoms. This interaction is attraction and so mobility of fluid particles decreases dramatically in vicinity of microchannel walls. By occur this atomic behavior, the fluid atoms disruption can be occured in the vicinity of the channel walls. Numerically, the maximum rate of this parameter of Ar/O_2 fluid occurs in middle bins of microchannel with 0.100/0.111 and 0.091/0.102 Å ps^{-1} rates for Pt microchannels from DPD and MD simulation methods, respectively. Similar atomic behavior estimated for Cu microchannel and maximum rate of Ar/O_2 fluid occur in middle bins with DPD/MD approach. As reported in Table 7, the maximum rate of Ar/O_2 fluid reaches to

Table 5 The maximum density of O_2/Ar fluid in Pt and Cu microchannel

	Pt microchannel	Cu microchannel
O_2 fluid-MD/atom/$Å^3$	0.039	0.033
O_2 fluid-DPD/Unit less	0.035	0.030
Ar fluid-MD/atom/$Å^3$	0.049	0.042
Ar fluid-DPD/Unit less	0.046	0.040

Table 6 The maximum density of O_2/Ar fluid in Pt and Cu nanochannels

	Pt nanochannel	Cu nanochannel
O_2 fluid-MD/atom/$Å^3$	0.028	0.024
O_2 fluid-DPD/Unit less	0.024	0.022
Ar fluid-MD/atom/$Å^3$	0.038	0.033
Ar fluid-DPD/Unit less	0.036	0.031

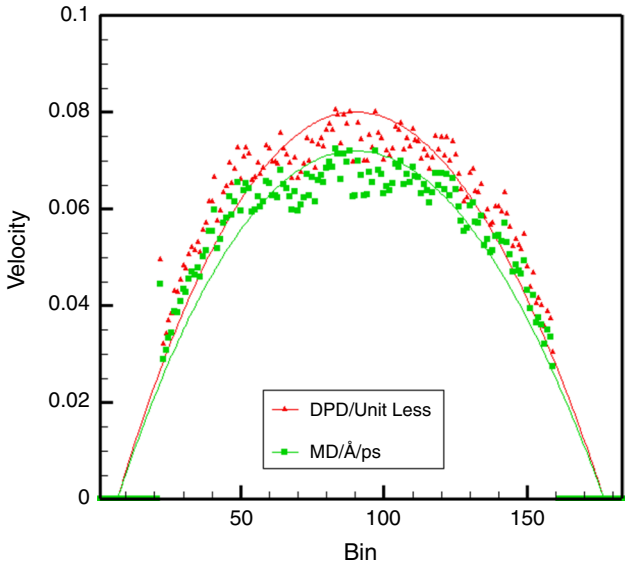

Fig. 8 Velocity profile of Ar fluid in Pt microchannel

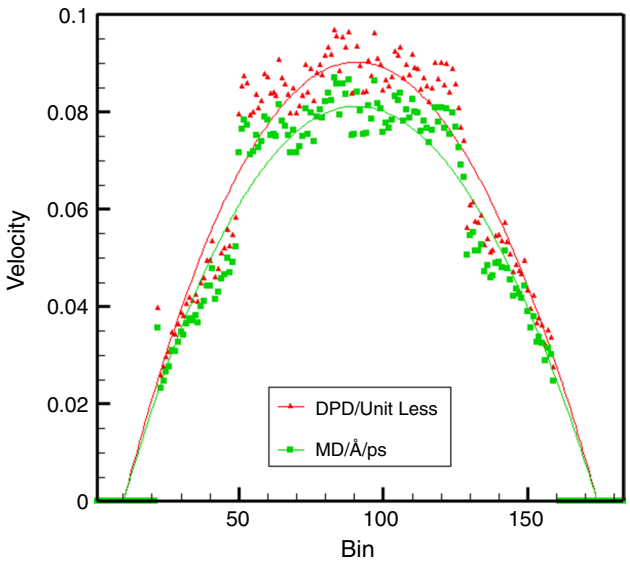

Fig. 9 Velocity profile of Ar fluid in Cu microchannel

Table 7 The maximum velocity of O_2/Ar fluid in Pt and Cu microchannels

	Pt microchannel	Cu microchannel
O2 fluid-MD/Å/ps	0.102	0.108
O2 fluid-DPD/Unit less	0.111	0.125
Ar fluid-MD/Å/ps	0.091	0.105
Ar fluid-DPD/Unit less	0.100	0.121

Table 8 The maximum velocity of O_2/Ar fluid in Pt and Cu nanochannels

	Pt nanochannel	Cu nanochannel
O_2 fluid-MD/Å/ps	0.092	0.099
O_2 fluid-DPD/Unit less	0.099	0.101
Ar fluid-MD/Å/ps	0.088	0.091
Ar fluid-DPD/Unit less	0.095	0.098

0.105/0.121 and 0.095/0.105 Å ps^{-1} rates in Cu channel, from stated methods, respectively. This atomic manner of fluids has practicable importance in thermodynamic mechanisms such as heat transfer procedures. By changing the channel size from micro to nanoscale, the maximum rate of Ar velocity reaches to 0.095/0.088 Å ps^{-1} for Pt nanochannel with DPD/MD simulation method for Ar fluid. Tables 7 and 8 report the maximum rate of fluid atoms in Pt/Cu channels estimated by various computational methods. From these calculated ratios, we can conclude that atomic fluids in Pt channels have maximum stability and so the fluid in this structure has minimum rate of atomic velocity. By decreasing the velocity, the time for phase transition increases which can be disrupted the thermal conductance procedure.

Temperature profile of atomic structures

In various structures such as atomic fluids, the temperature of fluid is appropriate with velocity of them. Theoretically, the relation between temperature and velocity of simulated structures is described by $\frac{1}{2}mv^2 = \frac{3}{2}kT$. In our computational work, this physical manner is verified exactly by this relation. Figures 10 and 11 show the temperature profile of Ar/O_2 fluid structure in Pt and Cu microchannels as a function of simulation method, respectively. As depicted in this figure, the Poiseuille flow has a quadratic temperature profile and the maximum rate of temperature for Ar fluid is 448/403 K and 485/436 K for Pt and Cu microchannels, which is predicted by DPD/MD method. O_2 fluid temperature behavior is similar to O_2 fluid as reported in Table 9. From our calculations for nanochannels, we can conclude that the profile of fluid temperature decreases by converting channel size from micro to nanosize. These phenomena occur from atomic distance decreasing by decreasing of channel size (Fig. 11; Table 10). Numerically, the maximum rates of fluid temperature occur in 91 and 92 bins for Pt and Cu nanochannels, respectively. The results of this section of calculations show

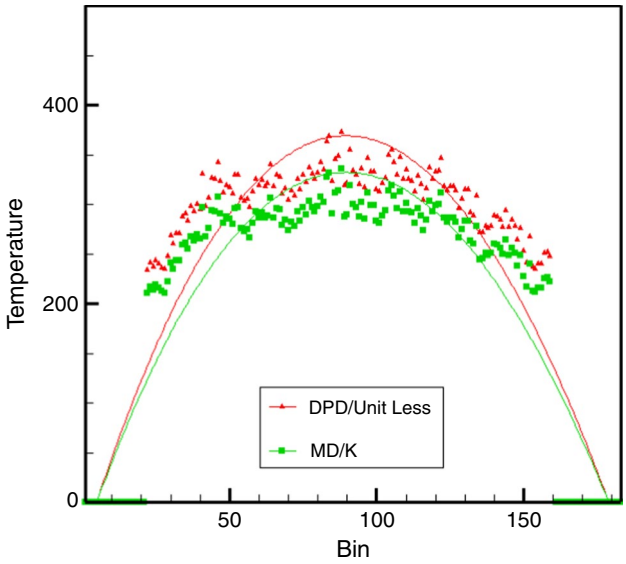

Fig. 10 Temperature profile of Ar fluid in Pt microchannel as a function of simulation method

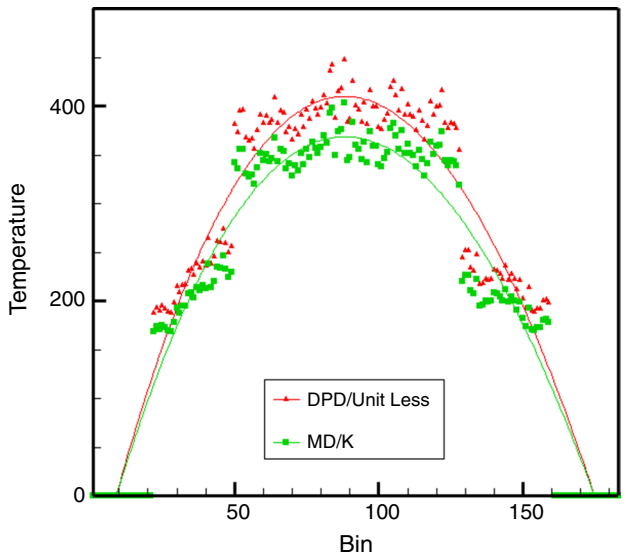

Fig. 11 Temperature profile of Ar fluid in Cu microchannel as a function of simulation method

Table 9 The maximum temperature of O2/Ar fluid in Pt and Cu microchannels

	Pt microchannel	Cu microchannel
O2 fluid-MD/K	421	446
O2 fluid-DPD/Unit less	455	499
Ar fluid-MD/K	403	436
Ar fluid-DPD/Unit less	448	485

Table 10 The maximum temperature of O_2/Ar fluid in Pt and Cu nanochannels

	Pt nanochannel	Cu nanochannel
O_2 fluid-MD/K	418	440
O_2 fluid-DPD/Unit less	449	485
Ar fluid-MD/K	398	416
Ar fluid-DPD/Unit less	442	481

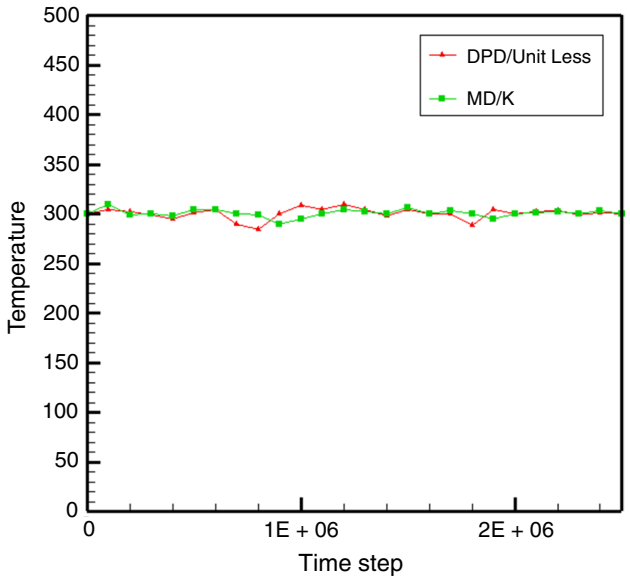

Fig. 12 Temperature of O_2–Ar mixture fluid ($\frac{1}{2}$: $\frac{1}{2}$) in Pt microchannel as a function of simulation method and time steps

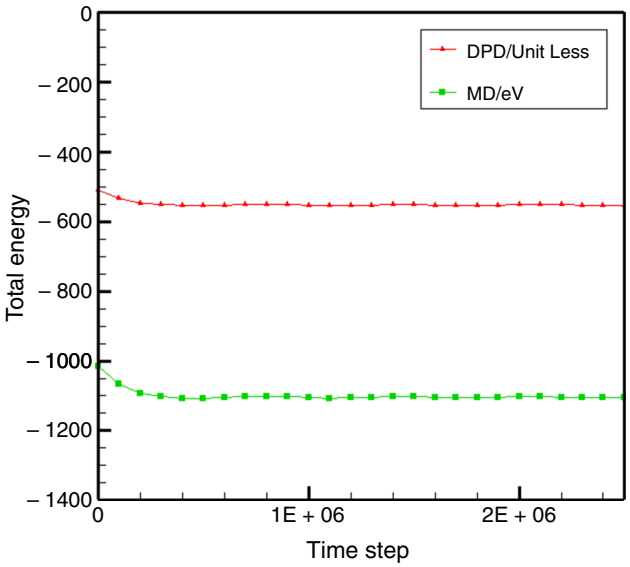

Fig. 13 Total energy of O_2–Ar mixture fluid ($\frac{1}{2}$: $\frac{1}{2}$) in Pt microchannel as a function of simulation method and time steps

the DPD and MD simulations ability to describe atomic fluid behavior in micro- and nano-structures.

Impact of Ar/O_2 atomic ratio on mixed fluid dynamical manner

In the final section of this work, we investigate the O_2 and Ar atomic ratio effects on dynamical manner of O_2–Ar mixture fluid. For atomic stability, analysis of this atomic mixture fluid in Pt microchannel, temperature, and total energy of fluid-channel system is reported. Figures 12 and 13 show the total temperature and total energy variation as a function of atomic rate of mixture fluids, respectively. As depicted in Fig. 13, the total energy of atomic structures numerically converged after 2,500,000 time steps by using DPD and MD approaches. Temperature of these structure show the similar manner and this thermodynamic parameter converged to 300 in 2,500,000 time steps. Further, total energy curve in this section shows that O_2–Ar mixture fluid total energy converged to bigger rate (magnitude) rather than pure fluids. Physically, by rising total energy magnitude rate, the stability of simulated structures rises. So we conclude that the O_2–Ar mixture fluid physical stability is bigger than each isolated fluids. Numerically, by adding Ar atoms to initial O_2 fluid by $\frac{1}{2}$, $\frac{1}{3}$, and $\frac{2}{3}$ rates, the total energy of simulated structures reaches to $-553/-1112$ eV, $-512/-1105$ eV, and $-502/-1087$ eV, respectively, by using DPD/MD approaches.

The density, velocity, and temperature profiles of O_2–Ar mixture fluid with various Ar atomic ratio ($\frac{1}{2}$, $\frac{1}{3}$, and $\frac{2}{3}$ rates) are reported in this section. Our DPD/MD simulations show that the maximum density of mixture fluid increases by increasing the Ar atomic ratio from 0.035/0.039 to 0.041/0.048 atom $Å^{-3}$. From Table 11, in our simulated microchannels, Cu one has the minimum density rate (0.031/0.033). This atomic manner shows that Ar atoms in mixture fluid interact with Pt atoms by maximum attraction force. Further, the maximum rate of mixture fluid velocity is calculated in middle bin of microchnnels and so we can say that by adding Ar atoms to O_2 base fluid, the Poiseuille flow

behavior can be detected with DPD and MD approaches. The velocity and temperature have direct relation with Ar atomic ratio in mixture fluid. By increasing the Ar atomic ratio, the oscillation of mixture fluid atoms decreases and so velocity of fluid structure decreases, too. Between our simulated structures, the maximum rate of atomic velocities is reported for Cu microchannel with 0.133/0.121 Å ps^{-1} from DPD/MD approaches as reported in Table 12. From relation between particle velocity and temperature, we can conclude that the temperature of mixture fluid decreases by increasing the Ar atomic ratio in simulation box. Numerically, maximum rate of mixture fluid temperature belongs to Cu microchannel with 489/448 K rate with DPD/MD approaches as reported in Table 13.

Table 13 The maximum rate of O_2/Ar mixture fluid atomic temperature in Pt and Cu microchannels as a function of Ar atomic ratio and simulation method

Ar atomic ratio—simulation method	Temperature in Pt microchannel	Temperature in Cu microchannel
$\frac{1}{2}$-MD/K	428	448
$\frac{1}{2}$-DPD/Unit less	473	489
$\frac{1}{3}$-MD/K	431	451
$\frac{1}{3}$-DPD/Unit less	475	493
$\frac{2}{3}$-MD/K	434	455
$\frac{2}{3}$-DPD/Unit less	478	499

Conclusions

In this computational study, we use dissipative particle dynamics and molecular dynamics approaches to describe the atomic manner of Ar, O_2 and mixture of these atomic fluids in Pt and Cu microchannel/nanochannel. In our simulations, the atomic ratio of Ar atoms in O_2–Ar mixture fluid varies from $\frac{1}{3}$ to $\frac{2}{3}$. From computational results, we conclude that the atomic ratio of each fluid and the type of simulated channel are being important parameters to structure the atomic and thermal behavior. Further, other results estimated from our computational study are given as follow:

a. The mixture fluid has the maximum atomic stability between various structures.
b. Fluid atomic mass is an important factor in density profile of O_2/Ar fluids. In our DPD/MD simulations, the maximum rate of density is calculated for Ar fluid in Pt microchannel with 0.046/0.049 atom $Å^{-3}$.
c. DPD/MD simulation results showed that by decreasing channel size, the maximum density of fluid decreases to 0.036/0.038 atom $Å^{-3}$.
d. In simulated structures, the velocity of fluids has reverse relation with Ar atomic ratio.
e. Maximum rate of atomic velocity is calculated for O_2 fluid in Cu microchannel with 0.125/0.108 Å ps^{-1} by using DPD/MD approach.
f. Maximum velocity rate of simulated fluids decreases to 0.101/0.099 Å ps^{-1} by simulated channels size decreasing from DPD/MD approach.
g. Temperature profile of simulated fluids increases by decreasing the Ar atoms ratio.
h. Maximum rate of atomic temperature is calculated for O_2 fluid in Cu microchannel with 499/446 K by using DPD/MD approach.
i. Decrease in microchannel size decreases the maximum rate of fluid temperature to 485/445 K in Pt channel by using DPD/MD approach

Finally, these calculated results show the DPD and MD method's ability in various fluid simulation atomic and thermal behavior. By comparing the results of MD and DPD simulations, we propose the use of DPD approach to study of large-scale simulations of fluid atomic manner in various conditions with very low computational cost. So this simulations method can be used for the optimization of various

Table 11 The maximum rate of O_2/Ar mixture fluid atomic density in Pt and Cu microchannels as a function of Ar atomic ratio and simulation method

Ar atomic ratio—simulation method	Density in Pt microchannel	Density in Cu microchannel
$\frac{1}{2}$-MD/atom/$Å^3$	0.048	0.033
$\frac{1}{2}$-DPD/Unit less	0.041	0.031
$\frac{1}{3}$-MD/atom/$Å^3$	0.043	0.030
$\frac{1}{3}$-DPD/Unit less	0.035	0.025
$\frac{2}{3}$-MD/atom/$Å^3$	0.041	0.028
$\frac{2}{3}$-DPD/Unit less	0.032	0.023

Table 12 The maximum rate of O_2/Ar mixture fluid atomic velocity in Pt and Cu microchannels as a function of Ar atomic ratio and simulation method

Ar atomic ratio—simulation method	Velocity in Pt microchannel	Velocity in Cu microchannel
$\frac{1}{2}$-MD/Å/ps	0.118	0.121
$\frac{1}{2}$-DPD/Unit less	0.125	0.133
$\frac{1}{3}$-MD/Å/ps	0.119	0.123
$\frac{1}{3}$-DPD/Unit less	0.128	0.135
$\frac{2}{3}$-MD/Å/ps	0.022	0.128
$\frac{2}{3}$-DPD/Unit less	0.129	0.136

fluid to reach maximum efficiency in various industrial applications such as thermal conductance, etc.

References

1. Bahiraei M, Jamshidmofid M, Goodarzi M. Efficacy of a hybrid nanofluid in a new microchannel heat sink equipped with both secondary channels and ribs. J Mol Liq. 2019;273:88–98.
2. Dadsetani R, Salimpour MR, Tavakoli MR, Goodarzi M, Bandarra Filho EP. Thermal and mechanical design of reverting microchannels for cooling disk-shaped electronic parts using constructal theory. Int J Numer Methods Heat Fluid Flow. 2019;30(1):245–65. https://doi.org/10.1108/HFF-06-2019-0453.
3. Sarafraz MM, Safaei MR, Goodarzi M, Yang B, Arjomandi M. Heat transfer analysis of Ga–In–Sn in a compact heat exchanger equipped with straight micro-passages. Int J Heat Mass Transf. 2019;139:675–84.
4. Sarafraz MM, Safaei MR, Goodarzi M, Arjomandi M. Experimental investigation and performance optimisation of a catalytic reforming micro-reactor using response surface methodology. Energy Convers Manag. 2019a;199:111983.
5. Sarafraz MM, Safaei MR, Goodarzi M, Arjomandi M. Reforming of methanol with steam in a micro-reactor with Cu–SiO_2 porous catalyst. Int J Hydrogen Energy. 2019b;44(36):19628–39.
6. Goodarzi M, Tlili I, Tian Z, Safaei MR. Efficiency assessment of using graphene nanoplatelets-silver/water nanofluids in microchannel heat sinks with different cross-sections for electronics cooling. Int J Numer Methods Heat Fluid Flow. 2019;30(1):347–72. https://doi.org/10.1108/HFF-12-2018-0730.
7. Li ZX, Khaled U, Al-Rashed AA, Goodarzi M, Sarafraz MM, Meer R. Heat transfer evaluation of a micro heat exchanger cooling with spherical carbon-acetone nanofluid. Int J Heat Mass Transf. 2020;149:119124.
8. Zheng Y, Zhang X, Soleimani Mobareke MT, Hekmatifar M, Karimipour A, Sabetvand R. Potential energy and atomic stability of H_2O/CuO nanoparticles flow and heat transfer in non-ideal microchannel via molecular dynamic approach: the Green-Kubo method. J Therm Anal Calorim. 2020. https://doi.org/10.1007/s10973-020-10054-w.
9. Mosavi A, Hekmatifar M, Alizadeh A, Toghraie D, Sabetvand R, Karimipour A. The molecular dynamics simulation of thermal manner of Ar/Cu nanofluid flow: the effects of spherical barriers size. J Mol Liq. 2020. https://doi.org/10.1016/j.molliq.2020.114183.
10. Asgari A, Nguyen Q, Karimipour A, Bach Q-V, Hekmatifar M, Sabetvand R. Investigation of additives nanoparticles and sphere barriers effects on the fluid flow inside a nanochannel impressed by an extrinsic electric field: a molecular dynamics simulation. J Mol Liq. 2020a. https://doi.org/10.1016/j.molliq.2020.114023.
11. Alrashed AA, Akbari OA, Heydari A, Toghraie D, Zarringhalam M, Shabani GAS, Seifi AR, Goodarzi M. The numerical modeling of water/FMWCNT nanofluid flow and heat transfer in a backward-facing contracting channel. Phys B. 2018;537:176–83.
12. Bahmani MH, Sheikhzadeh G, Zarringhalam M, Akbari OA, Alrashed AA, Shabani GAS, Goodarzi M. Investigation of turbulent heat transfer and nanofluid flow in a double pipe heat exchanger. Adv Powder Technol. 2018;29(2):273–82.
13. Abdulrazzaq T, Togun H, Goodarzi M, Kazi SN, Ariffin MKA, Adam NM, Hooman K. Turbulent heat transfer and nanofluid flow in an annular cylinder with sudden reduction. J Therm Anal Calorim. 2020;141:373–85. https://doi.org/10.1007/s10973-020-09538-6.
14. Yousefzadeh S, Rajabi H, Ghajari N, Sarafraz MM, Akbari OA, Goodarzi M. Numerical investigation of mixed convection heat transfer behavior of nanofluid in a cavity with different heat transfer areas. J Therm Anal Calorim. 2019;140:2779–803. https://doi.org/10.1007/s10973-019-09018-6.
15. Gheynani AR, Akbari OA, Zarringhalam M, Shabani GAS, Alnaqi AA, Goodarzi M, Toghraie D. Investigating the effect of nanoparticles diameter on turbulent flow and heat transfer properties of non-Newtonian carboxymethyl cellulose/CuO fluid in a microtube. Int J Numer Meth Heat Fluid Flow. 2019;29(5):1699–723. https://doi.org/10.1108/HFF-07-2018-0368.
16. Akbari OA, Safaei MR, Goodarzi M, Akbar NS, Zarringhalam M, Shabani GAS, Dahari M. A modified two-phase mixture model of nanofluid flow and heat transfer in a 3-D curved microtube. Adv Powder Technol. 2016;27(5):2175–85.
17. Hoogerbrugge PJ, Koelman JMVA. Simulating microscopic hydrodynamic phenomena with dissipative particle dynamics. Europhys Lett (EPL). 1992a;19(3):155–60. https://doi.org/10.1209/0295-5075/19/3/001.
18. Español P. Hydrodynamics from dissipative particle dynamics. Phys Rev E. 1995;52(2):1734–42. https://doi.org/10.1103/physreve.52.1734.
19. Satoh A, Majima T. Comparison between theoretical values and simulation results of viscosity for the dissipative particle dynamics method. J Colloid Interface Sci. 2005;283(1):251–66. https://doi.org/10.1016/j.jcis.2004.09.050.
20. Boek ES, Coveney PV, Lekkerkerker HNW, van der Schoot P. Simulating the rheology of dense colloidal suspensions using dissipative particle dynamics. Phys Rev E. 1997;55(3):3124–33. https://doi.org/10.1103/physreve.55.3124.
21. Schlijper AG, Hoogerbrugge PJ, Manke CW. Computer simulation of dilute polymer solutions with the dissipative particle dynamics method. J Rheol. 1995;39(3):567–79. https://doi.org/10.1122/1.550713.
22. Coveney PV, Novik KE. Computer simulations of domain growth and phase separation in two-dimensional binary immiscible fluids using dissipative particle dynamics. Phys Rev E. 1996;54(5):5134–41. https://doi.org/10.1103/physreve.54.5134.
23. Clark AT, Lal M, Ruddock JN, Warren PB. Mesoscopic simulation of drops in gravitational and shear fields. Langmuir. 2000;16(15):6342–50. https://doi.org/10.1021/la991565f.
24. Tiwari A, Abraham J. Dissipative particle dynamics simulations of liquid nanojet breakup. Microfluid Nanofluid. 2007;4(3):227–35. https://doi.org/10.1007/s10404-007-0166-3.
25. Tiwari A, Reddy H, Mukhopadhyay S, Abraham J. Simulations of liquid nanocylinder breakup with dissipative particle dynamics. Phys Rev E. 2008. https://doi.org/10.1103/physreve.78.016305.
26. Borhani M, Yaghoubi S. Numerical simulation of heat transfer in a parallel plate channel and promote dissipative particle dynamics method using different weight functions. Int Commun Heat Mass Transfer. 2020;115(104606):0735–1933. https://doi.org/10.1016/j.icheatmasstransfer.2020.104606.
27. Waheed W, Alazzam A, Al-Khateeb AN. Dissipative particle dynamics for modeling micro-objects in microfluidics. Biomech Model Mechanobiol. 2020;19:389–400. https://doi.org/10.1007/s10237-019-01216-3.
28. Ranjbarzadeh R, Moradikazerouni A, Bakhtiari R, Asadi A, Afrand M. An experimental study on stability and thermal conductivity of water/silica nanofluid: eco-friendly production of nanoparticles. J Clean Prod. 2019;206:1089–100.
29. Ranjbarzadeh R, Isfahani AM, Afrand M, Karimipour A, Hojaji M. An experimental study on heat transfer and pressure drop of water/graphene oxide nanofluid in a copper tube under air cross-flow: applicable as a heat exchanger. Appl Therm Eng. 2017;125:69–79.

30. Ranjbarzadeh R, Karimipour A, Afrand M, Isfahani AHM, Shirneshan A. Empirical analysis of heat transfer and friction factor of water/graphene oxide nanofluid flow in turbulent regime through an isothermal pipe. Appl Therm Eng. 2017;126:538–47.
31. Al-Rashed AA, Ranjbarzadeh R, Aghakhani S, Soltanimehr M, Afrand M, Nguyen TK. Entropy generation of boehmite alumina nanofluid flow through a minichannel heat exchanger considering nanoparticle shape effect. Phys A. 2019;521:724–36.
32. Ranjbarzadeh R, Akhgar A, Musivand S, Afrand M. Effects of graphene oxide-silicon oxide hybrid nanomaterials on rheological behavior of water at various time durations and temperatures: synthesis, preparation and stability. Powder Technol. 2018;335:375–87.
33. Frisch U, Hasslacher B, Pomeau Y. Lattice-gas automata for the Navier–Stokes equation. Phys Rev Lett. 1986;56(14):1505–8. https://doi.org/10.1103/physrevlett.56.1505.
34. Wolfram S. Cellular automaton fluids 1: basic theory. J Stat Phys. 1986;45(3–4):471–526. https://doi.org/10.1007/bf01021083.
35. Ladd AJC. Numerical simulations of particulate suspensions via a discretized Boltzmann equation. Part 2. Numerical results. J Fluid Mech. 1994;271:311. https://doi.org/10.1017/s002211209400178 3.
36. The finite element method for elliptic problems. Mathematics and computers in simulation. 1980;22(4):380. https://doi.org/10.1016/0378-4754(80)90078-6.
37. Spaid MAA, Phelan FR. Lattice Boltzmann methods for modeling microscale flow in fibrous porous media. Phys Fluids. 1997;9(9):2468–74. https://doi.org/10.1063/1.869392.
38. Lim CY, Shu C, Niu XD, Chew YT. Application of lattice Boltzmann method to simulate microchannel flows. Phys Fluids. 2002;14(7):2299. https://doi.org/10.1063/1.1483841.
39. Alder BJ, Wainwright TE. Studies in molecular dynamics. I. General method. J Chem Phys. 1959;31(2):459–66. https://doi.org/10.1063/1.1730376.
40. Rahman A. Correlations in the motion of atoms in liquid argon. Phys Rev. 1964;136(2A):A405–11.
41. Rapaport DC. The art of molecular dynamics simulation. 1996; ISBN: 0-521-44561-2.
42. Dehkordi KG et al. The electric field and microchannel type effects on H_2O/Fe_3O_4 nanofluid boiling process: molecular dynamics study. Int J Thermophys. (2020);41:132. https://doi.org/10.1007/s10765-020-02714-8.
43. Karimipour A, Malekahmadi O, Karimipour A, Shahgholi M, Li Z. Thermal conductivity enhancement via synthesis produces a new hybrid mixture composed of copper oxide and multi-walled carbon nanotube dispersed in water: experimental characterization and artificial neural network modeling. Int J Thermophys. 2020;41(8):1–27.
44. Asgari A, Nguyen Q, Karimipour A, Bach QV, Hekmatifar M, Sabetvand R. Develop molecular dynamics method to simulate the flow and thermal domains of H_2O/Cu nanofluid in a nanochannel affected by an external electric field. Int J Thermophys. 2020b;41(9):1–14.
45. Goel M, Harsha SP, Singh S, Sahani AK. Analysis of temperature, helicity and size effect on the mechanical properties of carbon nanotubes using molecular dynamics simulation. In: Materials today: proceedings; 2020.
46. Rappe AK, Casewit CJ, Colwell KS, Goddard WA, Skiff WM. UFF, a full periodic table force field for molecular mechanics and molecular dynamics simulations. J Am Chem Soc. 1992;114(25):10024–35. https://doi.org/10.1021/ja00051a040.
47. Lennard-Jones JE. On the determination of molecular fields. Proc R Soc Lond A. 1924;106(738):463–77. https://doi.org/10.1098/rspa.1924.0082.
48. Daw MS, Baskes M. Embedded-atom method: derivation and application to impurities, surfaces, and other defects in metals. Phys Rev B Am Phys Soc. 1984;29(12):6443–53. https://doi.org/10.1103/PhysRevB.29.6443.
49. Hoogerbrugge PJ, Koelman JMVA. Simulating microscopic hydrodynamic phenomena with dissipative particle dynamics. Europhys Lett. 1992b;19(3):155–60. https://doi.org/10.1209/0295-5075/19/3/001.
50. Koelman JMVA, Hoogerbrugge PJ. Dynamic simulations of hard-sphere suspensions under steady shear. Europhys Lett (EPL). 1993;21(3):363–8. https://doi.org/10.1209/0295-5075/21/3/018.
51. Español P, Warren P. Statistical mechanics of dissipative particle dynamics. Europhys Lett (EPL). 1995;30(4):191–6. https://doi.org/10.1209/0295-5075/30/4/001.
52. Goga N, Rzepiela AJ, de Vries AH, Marrink SJ, Berendsen HJC. Efficient algorithms for langevin and DPD dynamics. J Chem Theory Comput. 2012;8(10):3637–49. https://doi.org/10.1021/ct3000876.
53. Blumers A, Tang Y-H, Li Z, Li X, Karniadakis G. GPU-accelerated red blood cells simulations with transport dissipative particle dynamics. Comput Phys Commun. 2017;217:171–9. https://doi.org/10.1016/j.cpc.2017.03.016.
54. Tang Y-H, Li Z, Li X, Deng M, Karniadakis G. Non-equilibrium dynamics of vesicles and micelles by self-assembly of block copolymers with double thermoresponsivity. Macromolecules. 2016;49(7):2895–903. https://doi.org/10.1021/acs.macromol.6b00365.
55. Moeendarbary, et al. Dissipative particle dynamics: introduction, methodology and complex fluid applications—a review. Int J Appl Mech. 2009;1(4):737–63. https://doi.org/10.1142/S1758825109000381.
56. Sirk TW, Slizoberg YR, Brennan JK, Lisal M, Andzelm JW. An enhanced entangled polymer model for dissipative particle dynamics. J Chem Phys. 2012;136(13):134903. https://doi.org/10.1063/1.3698476.
57. Plimpton SJ, Thompson AP. Computational aspects of many-body potentials. MRS Bull. 2012;37(05):513–21. https://doi.org/10.1557/mrs.2012.96.
58. Brown WM, Wang P, Plimpton SJ, Tharrington AN. Implementing molecular dynamics on hybrid high performance computers—short range forces. Comput Phys Commun. 2011;182(4):898–911. https://doi.org/10.1016/j.cpc.2010.12.021.
59. Brown WM, Kohlmeyer A, Plimpton SJ, Tharrington AN. Implementing molecular dynamics on hybrid high performance computers—particle–particle particle–mesh. Comput Phys Commun. 2012;183(3):449–59. https://doi.org/10.1016/j.cpc.2011.10.012.
60. Stukowski A. Visualization and analysis of atomistic simulation data with OVITO—the open visualization tool. Modell Simul Mater Sci Eng. 2009;18(1):015012. https://doi.org/10.1088/0965-0393/18/1/015012.
61. Jolfaei NA, Jolfaei NA, Hekmatifar M, Piranfar A, Toghraie D, Sabetvand R, Rostami S. Investigation of thermal properties of DNA structure with precise atomic arrangement via equilibrium and non-equilibrium molecular dynamics approaches. Comput Methods Progr Biomed. 2019. https://doi.org/10.1016/j.cmpb.2019.105169.
62. Arani AAA, Akbari OA, Safaei MR, Marzban A, Alrashed AA, Ahmadi GR, Nguyen TK. Heat transfer improvement of water/single-wall carbon nanotubes (SWCNT) nanofluid in a novel design of a truncated double-layered microchannel heat sink. Int J Heat Mass Transf. 2017;113:780–95.
63. Ghanbari A, Warchomicka F, Sommitsch C, Zamanian A. Investigation of the oxidation mechanism of dopamine functionalization in an AZ31 magnesium alloy for biomedical applications. Coatings. 2019;9(9):584. https://doi.org/10.3390/coatings9090584.

64. Karimipour A, Jolfaei NA, Hekmatifar M, Toghraie D, Sabetvand R, Karimipour A. Prediction of the interaction between HIV viruses and human serum albumin (HSA) molecules using an equilibrium dynamics simulation program for application in bio medical science. J Mol Liq. 2020. https://doi.org/10.1016/j.molliq.2020.113989.
65. Zheng Y, Zhang X, Nouri M, et al. Atomic rheology analysis of the external magnetic field effects on nanofluid in non-ideal microchannel via molecular dynamic method. J Therm Anal Calorim. 2020. https://doi.org/10.1007/s10973-020-10191-2.
66. Heydari A, Akbari OA, Safaei MR, Derakhshani M, Alrashed A, Mashayekhi R, Shabani GAS, Zarringhalam M, Nguyen TK. The effect of attack angle of triangular ribs on heat transfer of nanofluids in a microchannel. J Therm Anal Calorim. 2018;131:2893–912.
67. Sabetvand R, Ghazi ME, Izadifard M. Studying temperature effects on electronic and optical properties of cubic $CH_3NH_3SnI_3$ perovskite. J Comput Electron. 2020;19:70–9. https://doi.org/10.1007/s10825-020-01443-3.
68. Ashkezari AZ, Jolfaei NA, Jolfaei NA, Hekmatifar M, Toghraie D, Sabetvand R, Rostami S. Calculation of the thermal conductivity of human serum albumin (HSA) with equilibrium/non-equilibrium molecular dynamics approaches. Comput Methods Programs Biomed. 2019. https://doi.org/10.1016/j.cmpb.2019.105256.
69. Dadsetani R, Sheikhzadeh GA, Hajmohammadi MR, Safaei MR. Introduce a novel configurationof microchannel andhigh-conductivity insertsfor cooling of disc-shaped electronic components. Int J Numer Meth Heat Fluid Flow. 2019;30(6):2845–59. https://doi.org/10.1108/HFF-02-2019-0105.
70. Hekmatifar M, Toghraie D, Khosravi A, Saberi F, Soltani F, Sabetvand R, Shahsavar GA. The study of asphaltene desorption from the iron surface with molecular dynamics method. J Mol Liq. 2020;114325:0167–7322. https://doi.org/10.1016/j.molliq.2020.114325.
71. Qi C, Wang G, Yang L, Wan Y, Rao Z. Two-phase lattice Boltzmann simulation of the effects of base fluid and nanoparticle size on natural convection heat transfer of nanofluid. Int J Heat Mass Transf. 2017;105:664–72.
72. Qi C, Tang J, Wang G. Natural convection of composite nanofluids based on a two-phase lattice Boltzmann model. J Therm Anal Calorim. 2020;141:277–287.
73. Jalali E, Ali Akbari O, Sarafraz MM, Abbas T, Safaei MR. Heat transfer of oil/MWCNT nanofluid jet injection inside a rectangular microchannel. Symmetry. 2019;11(6):757.
74. Qi C, Yang L, Wang G. Numerical study on convective heat transfer enhancement in horizontal rectangle enclosures filled with Ag–Ga nanofluid. Nanoscale Res Lett. 2017;12(1):326.
75. Qi C, Liang L, Rao Z. Study on the flow and heat transfer of liquid metal based nanofluid with different nanoparticle radiuses using two-phase lattice Boltzmann method. Int J Heat Mass Transf. 2016;94:316–26.
76. Noorian H, Toghraie D, Azimian AR. Molecular dynamics simulation of Poiseuille flow in a rough nano channel with checker surface roughnesses geometry. Heat Mass Transf. 2013;50(1):105–13. https://doi.org/10.1007/s00231-013-1232-x.
77. Maknickas A, Skarbalius G, Džiugys A, Misiulis E. Nanoscale water Poiseuille flow: MD computational experiment. In: 3rd National conference on current and emerging process technologies—concept 2020; 2020. https://doi.org/https://doi.org/10.1063/5.0007798.
78. Jiang Y, Dehghan S, Karimipour A, Toghraie D, Li Z, Tlili I. Effect of copper nanoparticles on thermal behavior of water flow in a zig-zag nanochannel using molecular dynamics simulation. Int Commun Heat Mass Transfer. 2020;116:104652. https://doi.org/10.1016/j.icheatmasstransfer.2020.104652.
79. Huang Y, Marson RL, Larson RG. Inertial migration of neutrally buoyant prolate and oblate spheroids in plane Poiseuille flow using dissipative particle dynamics simulations. Comput Mater Sci. 2019;162:178–85. https://doi.org/10.1016/j.commatsci.2019.02.048.